New synthesis routes and catalytic applications of ferrierite crystals. Part 1: 1,8-Diaminooctane as a new OSDA

Enrico Catizzone, Massimo Migliori, Tzonka Mineva, Stijn van Daele, Valentin Valtchev, Girolamo Giordano

New synthesis routes and catalytic applications of ferrierite crystals. Part 1: 1,8-diaminooctane as a new OSDA

Enrico CATIZZONE [a], *Massimo MIGLIORI** [b], *Tzonka MINEVA* [c], *Stijn van DAELE* [d], *Valentin VALTCHEV* [e] *and Girolamo GIORDANO* [b]

[a] ENEA-Italian National Agency for New Technologies, Energy and Sustainable Economic Development, Trisaia Research Centre, I-75026, Rotondela (MT), Italy.

[b]University of Calabria, Department of Environmental and Chemical Engineering, Via P. Bucci – I-87036 Rende (CS), Italy.

[c] Matériaux Avancés pour la Catalyse et al Santé, UMR 5253 CNRS/UM/ENSCM, Institut Charles Gerhardt de Montpellier (ICGM), 240, Avenue du Professeur Emile Jeanbrau, 34296, Montpellier cedex 5, France.

[d] Total Research and Technology Feluy (TRTF), Zone Industrielle C, 7181 Feluy, Belgium.

[e] Laboratoire Catalyse et Spectrochimie CNRS, ENSICAEN, Université de Caen Basse-Normandie, 6 Boulevard Maréchal Juin, Caen, France

*Corrisponding author email : massimo.migliori@unical.it

* Corresponding author
Email: massimo.migliori@unical.it
Telephone: +39 0984496641

ABSTRACT

Ferrierite zeolite crystals were successfully prepared by a long amine as 1,8-diaminoctane (DAO) as organic structure directing agent. By comparison, shorter amine, i.e. ethylenediamine (EN), was also used as OSDA. Results shows that the presence of DAO reduces the crystallization time and allows to obtain single FER-type crystlas with smaller size and higher acidity, being these significant parameters to take into account when zeolites are applied in catalysis. The obtained samples were characterized with XRD, TG/DTA, SEM, N_2 adsoprtion/desorption, FTIR and ^{27}Al-NMR. In particular, TGA clearly shows that DAO may be accommodate in zeolite framework and theoretical modeling suggests a preferential location in the 10-MR ring channels.

Keywords: Ferrierite, zeolite synthesis, 1,8-diaminooctane, Brønsted-Lewis acidity, FT-IR, DFT calculation,

1. INTRODUCTION

The possibility of preparing zeolites with tailored physicochemical properties by both in situ and post-synthesis treatments is of considerable importance for the industrial perspective, particularly in the area of heterogeneous catalysis where zeolites are widely used [1-6]. In fact, the suitability of zeolite for specific applications, such as catalysis, strongly depend on several factor such as zeolite structure (i.e. size, shape and orientation of the channels), its chemical composition, acidity and crystal morphology. At moment, more than 240 zeolite framework types are known and most of them are not currently applied in industrial processes due to both costs and performances aspects, and

very few zeolite structures have found significant catalytic application in petrochemical and refining industries. FAU (X and Y), MFI (ZSM-5 and Silicalite-1), MOR, BEA (beta), MWW (MCM-22), AEL (SAPO-11) and CHA (SAPO-34) are examples of zeolite structures currently used in industrial catalysis.

Ferrierite (FER) is another zeolite structure that has or may have some importance for industrial applications. FER framework consists of an intersecting 2-dimensional system of 10- (5.4 x 4.2 Å) and 8- (4.8 x 3.5 Å) member ring channels and can by synthesised with Si/Al ratios ranging from 5 to infinity [8, 9]. The particular channel configuration of FER framework is appropriate for processing small molecules. For instance, FER-type zeolite is mainly applied as catalyst in the skeletal isomerization of n-butene for the production of iso-butene and as additive to ZSM-5 catalyst in the dewaxing by selective cracking process for the production of lubricant [10]. Recently, FER-type crystals have also ranked as a highly performing catalyst for dimethyl ether (DME) production via both methanol dehydration reaction and one-pot CO or CO_2 hydrogenation, if compared with other zeolite structures such as MFI, BEA, MOR, CHA, MTW and TON [11-14]; the superiority of ferrierite over the traditional catalyst for DME synthesis, i.e. γ-Al_2O_3, was also reported [15].

Ferrierite can be synthesized combining both Na^+ and K^+ cations [16]. However, it is usually obtained from sodium and OSDA containing systems which give more flexibility in the control of the physicochemical properties of the ultimate product. Amines are often used as OSDA in the synthesis of FER-type materials. Göğebakan et al. [17] reported a study on crystallization field and rate in presence of pyrrolidine or ethylenediamine in the synthesis temperature range 150-225 °C, founding a strong dependence of crystallization rate from temperature, whereas both SiO_2/Al_2O_3 ratio (in

the range 10-25) and OSDA amount did not significantly influence the crystallization rate. On the contrary, OSDA affected crystal morphology: individual or platelet crystallites were obtained in presence of pyrrolidine or ethylenediamine, respectively. Furthermore, the authors even found mordenite as competitive phase only when pyrrolidine is used as OSDA.

Kamimura et al. [9] reported the synthesis of ferrierite in presence of pyridine as OSDA, obtaining well-defined plate-like crystals with a SiO_2/Al_2O_3 up to 324. In particular, the synthesis of pure siliceous ferrierite was successful in presence of sodium fluoride. Aluminium-free ferrierite was also obtained in presence of ethylediamine as OSDA and boric acid as templates [18].

On the contrary, Forbes et al. [19] reported that, using diethanolamine as OSDA, pure phase ferrierite crystals may be obtained only in a narrow Si/Al ratio. In particular, the authors found that by increasing the SiO_2/Al_2O_3 from 16 to about 25, a ferrierite/ZSM-5 mixed phase was obtained.

OSDA type as well as synthesis environment also affects the morphology and the size of the final crystals. In this concern, Rakozy et al. [20, 21] report the synthesis of all-silica large FER-type crystals by using unbranched monoalkyl C3-C5 amines in mixture with pyridine, showing the possibility to tune the shape and size of obtained crystals. In particular, by increasing the number of carbon atoms of the amine, the crystal shape changed from hexagonal to rectangular flat prismatic morphology.

Lee et al. [22] successfully synthesised ferrierite zeolite nanoneedles about 10 nm in diameter and 100 nm in length. The success of the synthesis strongly depends on both Si/Al ratio and ion types. In particular, the authors obtained high pure ferrierite by

adopting a Si/Al=20 in presence of Na+, while mixed or amorphous phases were obtained for lower or higher aluminium content and using other ion types (e.g. Li^+, K^+, Rb^+, Cs^+).

The effect of organic solvent such as triethylamine, tetra- or diethylene glycole, dimethylsulfoxide, lutidine and mineral oil on the shape and size of final crystals from non-aqueous syntheses was also deeply investigated [23].

Pinar et al. assert that the choice of organic template molecules (OSDA) in FER-type materials is of paramount importance for aluminium distribution and incorporation [23], affecting acid sites distribution, location, and accessibility [24]. The authors synthesised ferrierite crystals with a Si/Al ratio of about 15 starting from a sodium-free gels in fluoride media by using some specific combinations of tetramethylammonium (TMA), pyrrolidine and benzylmethylpyrrolidinium (bmp), founding that the acid sites distribution between the ferrierite cage accessible to through 8-MR window and the 10-MR pores depend on the OSDA mixture composition. In particular, the accessibility to Brønsted sites is higher when TMA/bmp or TMA/pyrrolidine mixture are used respected to alone pyrrolidine with a direct effect on catalysis. Therefore, the already published studies highlighted the possibility to obtain tailored ferrierite crystals by choosing proper SDAs and synthesis conditions, with an effective control of both acid properties and crystal morphology.

In this paper, FER-type crystals were synthesized by using a long amine as 1,8-diaminooctane as OSDA. This molecule is usually used for the synthesis of MEL, TON and ZSM-48 zeolites. In the case of MEL and TON zeolite, the success of the crystallization of the desired phase strongly depends on the stirring condition: static or high-speed agitation condition lead to the selective formation of high pure MEL or TON

phase, respectively [25]. Crystallization with stirring is also required for the synthesis of ZSM-48 [26].

To the best of our knowledge, there has been no report on the synthesis of ferrierite by using 1,8-diaminoctane as OSDA. In this work the crystallization of ferrierite in presence of 1,8-diaminioctane is carried out with the aim to assess the effect of this molecule on physico-chemical properties of obtained materials. Furthermore, in order to have new insights about the role of amine molecule length, FER-type zeolite with ethylenediammine as OSDA was also prepared for comparison.

TG/DTA analysis allowed to assess the interaction between the OSDA and zeolite framework whilst DFT calculations gave information about molecules location. Brønsted/Lewis acid sites distribution and concentration of synthesised materials have been investigated with NH_3-TPD and FT-IR of several adsorbed probe molecules while morphology and crystallinity has been analysed by scanning electron microscopy and powder XRD, respectively. Finally, DFT calculations allowed validate the experimental evidences.

2. EXPERIMENTAL

2.1 Samples preparation

The following chemicals were used in all the synthesis: colloidal silica Ludox AS-40 (SiO_2, 40 wt% suspension in H_2O, Aldrich), sodium aluminate ($NaAlO_2$, Aldrich), sodium hydroxide (pellets, Aldrich), ethylenediamine (Fluka), 1,8-diaminooctane (Aldrich), and distilled water.

Synthesis of FER sample by using ethylenediamine (En-FER) was prepared by adopting the following synthesis gel molar composition [28]:

$$19.7\ En - 1.85\ Na_2O - 15.2\ SiO_2 - 1\ Al_2O_3 - 590\ H_2O$$

In a typical synthesis 0.3 g of NaOH and 1.3 g of sodium aluminate were dissolved in 64.1 g of distilled water. Then 8.2 g of ethylenediamine were added to dropwise and the solution was stirred for 30 min. Afterwards 15.8 g of colloidal silica were added dropwise to the solution, and the obtained gel was stirred (300 rpm) at room temperature for 1 h. Crystallization was carried out in 120 ml stainless-steel Teflon coated autoclave up to 12 days at 180 °C in a tumbling oven (rotation speed: 15 rpm).

The potential role of 1,8-diaminooctane as OSDA was investigated by gradually replacing En with DAO, starting from the En-FER (i.e. DAO free) synthesis gel. FER-type crystals were obtained from synthesis gel with different DAO/En molar ratio: 0.25, 0.5, 1, 2 and ∞ (i.e. En free), by using the following molar gel composition

$$x\ DAO - 1.85\ Na_2O - 15.2\ SiO_2 - 1\ Al_2O_3 - 590\ H_2O - y\ En$$

with $5<x<10$ and $0<y<19.7$.

In the synthesis of DAO-FER only DAO was used as SDA. For this latter synthesis, 0.3 g of NaOH and 1.3 g of sodium aluminate were dissolved in 21 g of distilled water. A secondary solution was prepared by dissolving 7.8 g of DAO into 42 g of distilled water, under vigorous stirring. Afterwards, the two solutions were blended and 15.8 g of colloidal silica were added dropwise and the obtained gel was stirred (300 rpm) at room temperature for 1 h. Crystallization was carried out in 120 ml stainless-steel Teflon coated autoclave up to 12 days at 180 °C in a tumbling oven (rotation speed: 15 rpm).

After crystallization, the solid was separated by vacuum filtration and washed several times with distilled water until the pH of filtered solution was close to the neutral value. The obtained white solid was then dried for 15 hours in a static oven kept at 80 °C. In order to remove template from zeolite, air-flow calcination was carried out at 550 °C with an holding time of 8 hours and a heating rate of 2 °C/min. Afterwards, H-form solid was obtained by ion-exchange with a NH_4Cl 1 M solution at 80 °C followed by a secondary air-flow calcination at 550 °C with an holding time of 8 hours and a heating rate of 2 °C/min [29].

2.2 Physicochemical characterization

X-Ray powder diffraction (APD 2000 Pro) (region $5° < 2\theta < 50°$, step 0.02°/ s) was used to verify both purity and crystallinity of obtained phase; the morphology of the crystalline phase was observed on a scanning electron microscope (SEM, FEI model Inspect) and a transmission electron microscopy (TEM, Philips CM12). The sodium, aluminum and silicon content in the calcined catalysts was measured by atomic absorption spectroscopy (GBC 932 AA).

The specific surface area and the micropores volume of the calcined samples were obtained from BET and t-plot analysis of porosimetry data (ASAP 2020 Micromeritics) under nitrogen adsorption at -196 °C, after a pre-treatment in vacuum at 200°C for 12 h. The thermo-gravimetric analysis over the as-synthesised samples was performed on the automatic TG/DTA instrument (Shimadzu) under 50 cc/min of air flow in the temperature range 25-850°C (heating rate of 5 $°C \cdot min^{-1}$).

Solid-state magic angle spinning nuclear magnetic resonance spectroscopy (MAS-NMR) was used to characterize the local ^{27}Al environment in the zeolite samples. All data were recorded on a Bruker Advance 500 MHZ spectrometer using a 4.0 mm rotors.

The ^{27}Al-NMR spectra were acquired at 130.3 MHz with radiofrequency power of 54 kHz, a pulse length of 4.6 μs with a corresponding angle theta of π/4. Rotors were spun at 14 kHz, and the recycle delay used for both nuclei was 1 second.

Surface acidity of H-form sample was measured by NH_3-TPD analysis (TPDRO1100, ThermoFisher) according to the following procedure. Dried sample (100 mg, pellet mesh 90-150 μm) was loaded in a linear quartz micro-reactor and pre-treated at 300°C in helium flow for 1 h to remove adsorbed water. The sample was cooled down to 150°C and saturated with 10% v/v NH_3/He mixture with a flow rate of 20 STP mL·min^{-1} for 2 h. Ammonia physically adsorbed was removed by purging in helium at 150°C for 1 h until TCD baseline stabilization. Desorption measurement was carried out in the temperature range of 100-950°C (10 °C·min^{-1}) using a helium flow rate of 20 STP mL·min^{-1}.

Brønsted and Lewis acid sites concentration was measured via FT-IR analysis by using D_3–acetonitrile as a probe molecule. Infrared spectra were recorded with a Bruker Equinox 55 spectrometer. The adsorption of D_3–acetonitrile was performed at room temperature with a pressure of 10 Torr, after that the samples were degassed under high vacuum condition (cell pressure: 10^{-6} Torr) at 300°C for 4 h, in order to purge adsorbed water. Physisorbed acetonitrile was removed by further degassing until the vacuum condition was recovered. The FT-IR spectra were recorded in the temperature range 25-300 °C (temperature step of 50°C), outgassing the sample for 30 minutes at any temperature variation.

The amount of D_3–acetontrile adsorbed on Brønsted and Lewis was determined by using a literature value for the molar absorption coefficient [30]. The number of Brønsted sites was calculated from the area of the bands observed at 2297 cm^{-1} by

adopting an extinction coefficient of 2.05 cm/μmol, whilst the number of Lewis acid sites was calculated from the area of the bands between 2310–2325 cm^{-1} by adopting an extinction factor of 3.6 cm/μmol. Peaks analysis and deconvolution for both FT−IR and NH_3-TPD profiles were performed by using commercial software (PeakFit 4.12, Seasolve−USA).

3. RESULTS AND DISCUSSION

3.1 Structural properties of FER-type zeolites synthesized with different OSDA

X-ray patterns as a function of crystallization time of En-FER and DAO-FER are reported in Figure 1. Crystal growth kinetics of En-FER is relatively slow (see Figure 1-A) as traces of FER phase are observed after 3 days and after 6 days the crystalline phase is dominant. A crystallization time of 10 days can be considered as optimal to obtain high crystalline En-FER since, for longer time (12 days), traces of kaetite phase appear. Figure 1-B reports the XRD patters as a function of crystallization time for DAO-FER sample. Results show that En replacing with DAO speeds the crystallization. In fact, after 3 days FER-phase is almost completely crystallized whilst only traces of crystalline product are observed for En-FER after the same synthesis period. That evidence suggests that in presence of DAO, the induction period is shortened, even reducing the crystal size as discussed later.

Because DAO was never reported as a template in FER zeolite synthesis, a deeper investigation by TG/DTA analysis of as-synthesised materials was performed. The thermo-analytic results of DAO-containing systems are reported in Figure 2, in terms of

thermogravimetric (TG) and first derivate (dTG) profiles. Heat flow profiles (DTA) are reported in Figure S.1 (Supporting Information).

From the analysis of the dTG profiles, it can be deducted that 1,8-diaminooctane might plays the role of template for FER structure. In fact, dTG profile of DAO-free sample (En-FER, Figure 2A) shows the presence of four main peaks [28]. The endothermic peak (see Figure S.1A) at ca. 73 °C is attributed to water release and the corresponding weight loss for En-FER was of ca. 2 wt%. In addition, En-FER sample contains about 11 wt% of ethylendiammine, released in the temperature range 250-700 °C. The associated exothermic phenomena (see DTA profile reported in Figure S.1A) are related to the organic combustion. It is evident from Figure 1A, that at least four different dTG peaks can be associated to ethylenediamine decomposition (249°C, 302 °C, 420 °C and 605 °C), indicating the presence of different interactions between OSDA and zeolite framework. As the DAO/En ratio increases from 0 to 0.5 or 1 an effect of a shift toward low temperatures is observed for these dTG peaks. If the peak of En-FER at 420° C is considered, it clearly appears that it decreases down to 366 °C and 352 °C (Figures 2B-C) when the DAO/En ratio is increased to 0.5 or 1, respectively. Also, dTG profile reported in Figure 2C shows that the interaction between ethylenediamine and zeolite framework characterised by the lowest temperature decomposition (around 249°C for En-FER) tends to disappear when DAO progressively replaces En as OSDA. It is worthy to clarify that this effect it is not attributable to lower amount of En in synthesis gel because the TG/dTG profile of a DAO-free FER synthesised with the same ethylenediamine content of the sample with DAO/En=2 (i.e. En/Al_2=5) shows the same peaks of the En-FER (En/Al_2=19.7), as reported in Figure S.2 of Supporting information. This result suggests that the amount of ethylediamine in the synthesis gel

slightly affects its incorporation and the changing of dTG profiles that are, on the contrary, mainly affected by the presence of DAO in the synthesis gel and then in the zeolite structure. The effect of the only DAO in the FER synthesis is shown in Figure 2.D, where the main exothermic peak at 348 °C can be unequivocally attributed to 1,8-diaminooctane combustion. The weight loss due to organic molecules decomposition, measured in the temperature range 250-650 °C decreases from ca. 11 wt% to ca. 7 wt% when the DAO/En ratio increases from 0 to ∞ respectively. On the contrary, the weight loss between 25 and 200 °C, attributed to physically adsorbed water, increase from 2 wt% to 5 wt % by increasing the DAO/En ratio from 0 to ∞, respectively, suggesting that the presence of 1,8-diaminooctane also promotes the water incorporation. Even though the role and the location of DAO molecules is not fully elucidated yet, we anticipate that DAO molecules are located inside the 10 MR of FER structure since the 8 MR channel is too small to accommodate them.

Figure S.3 shows the ^{27}Al MAS NMR spectra of the H-form FER-type zeolites with En or DAO as OSDA. They are dominated by a signal centered at around 55 ppm, characteristic of tetra-coordinated aluminium species in zeolite framework. A broad signal at around 0 ppm revealing the presence of octahedral extra-framework aluminium (about 10%) for both the samples. The observed quadrupolar line broadening can be caused by distortions of the octahedral symmetry of AlO_6 sites.

It is well-known that the zeolite structure is generated by a network of SiO_4 and AlO_4^- tetrahedral linked together by a shared oxygen atom. Due to the presence of trivalent atoms (e.g. aluminium) in the tetrahedral units, the framework offers a negative charge which needs to be balanced with non-framework exchangeable cations that are generally elements of the group IA and group IIA as sodium, potassium, magnesium

and calcium. In this work, sodium is used to synthesise FER-type materials, and this is the cation that balances negative charges associated with aluminium atoms. Furthermore, the high quantity of tetrahedral aluminium species detected by NMR analysis, suggests that the Na/Al ratio should be theoretically around one. The chemical analysis reported in Table 1 shows that Na/Al is 0.06 for En-FER and 0.6 for DAO-FER. These results disagree with the previous theoretical assumption, suggesting that sodium cations do not balance an important amount of aluminium species in tetrahedral position, expecially. Vuono et al. [31] reported a Na/Al ratio value below to unity (around 0.6) for MCM-49 materials synthesised in the presence of hexamethylenimine despite aluminium was mainly tetra-coordinated as in our case. Forbes et al. [32, 33] report that during the synthesis of ZSM-5/Theta-1 materials in the presence of diethanolammine, the organic molecules were considered to have both a pore-filling role and charge compensatory role. Furthermore, Rollmann et al. [34] assert that protonated amine (e.g. ethylamine, pyrrolidine, hexamethylenimine) play the role as counter ion of negative charge associated to tetrahedral aluminium atoms located into zeolite framework, also for FER-type materials. Therefore, because in this work, aluminium atoms are mainly present in tetrahedral coordination, protonated organic molecules can be reasonably present to compensate negative charge of zeolite lattice. Therefore, theoretically the $(OSDA^{+}+Na^{+)}/AlO_2^{-}$ molar ration should be about one in order to have the balance of aluminium negative charge. In this regard, it is possible to calculate the unit cell molar composition for En-FER and DAO-FER, respectively, as it follows:

En-FER: $En_{3.9}Na_{0.2}Al_{3.8}Si_{32.2}O_{72}\cdot 2.8\ H_2O$

DAO-FER: $DAO_{1.0}\ Na_{2.8}Al_{4.7}Si_{31.3}O_{72}\cdot 7.8\ H_2O$

Results clearly show that ethylenediamine is able to compensate the aluminium negative charge of zeolite framework since En^{+}/AlO_2^{-} molar ration is near one and a negligible sodium amount is incorporated. On the contrary, 1,8-diaminooctane is not able to compensate all of the aluminium negative charge and a higher amount of sodium is incorporated. Moreover, in order to respect the electro-neutrality of the framework, one DAO molecule should be able to compensate two aluminium negative charge. This condition may be obtained if both the amino groups of DAO molecules are protonated and able to compensate two different aluminium negative charge. This statement is also confirmed by DFT theoretical study later reported.

The results of N_2 adsorption analysis are summarized in Table 1. En-FER sample shows a slightly higher micropore volume than DAO-FER sample. This difference may be related to the sodium content.

Figure 3 shows the adsorption/desorption isotherms of synthesised samples in protonic form. Both En-FER and DAO-FER sample exhibit a type I adsorption isotherms typical of microporous materials [28] but some differences may be highlighted. In fact, for En-FER sample an uptake increase is observed at $P/P°>0.9$, that is less evident for DAO-FER sample. This isotherm shape of En-FER may indicate the presence of external mesopores due to agglomeration of crystals, as also revealed by SEM.

Figure 4 shows representative SEM micrographs reveailing that all samples exhibit the typical of ferrierite plat-like morphology with a well-developed {1 0 0}. However, the crystals differ in size and the level of agglomeration. The En-FER crystals (Figure 6A) have the following characteristics: length 2-3 µm, length/width ratio around 2 and thickness 100 nm, while DAO as OSDA generates smaller crystals with size below 1 µm and lower length/width ratio (around 1.3). As showed by XRD analysis, a higher

crystallization rate is observed for DAO-FER sample, that may cause the formation of smaller crystals. Moreover, a significant agglomeration is observed for En-FER sample, while single crystal is obtained in presence of DAO.

3.2 Zeolite acidity

The NH_3-TPD profiles are reported in Figure 5 for all the synthesised samples displaying three main peaks characterised by different ammonia maximum desorption temperatures peaks (T_M) as an indicator of different acid sites family (the higher is T_M, the stronger is the acid sites).

As suggested by Niwa and Katada [35, 36], the interpretation of peaks with T_M<300 °C may be quite misleading since the desorption effect may also be related to physically adsorbed ammonia interacting via a hydrogen bond with the NH_4^+ ions adsorbed onto acid sites. In this condition, having comparable desorption energy, the presence of weak acid sites, may be partially hidden by physisorbed ammonia. On the contrary, the peaks with 300°C<T_M<500 °C are associated with ammonia molecules desorbed from strong acid sites (both Brønsted and Lewis acid sites). The peak with T_M>700 °C can be associated to dehydroxylation phenomena [37, 38] since it is detected either in NH_3-TPD experiments or in the corresponding "blank" TPD experiments performed over the same catalyst and under the same experimental conditions, without NH_3 feed.

Quantitative results of NH_3-TPD measurements reported in Table 2. DAO-FER sample exhibits a higher total acid sites concentration according to the higher aluminium content measured by atomic absorption technique. DAO-FER also shows a higher $T_{M,HT}$ indicating a major strength of acid sites. Such aspect may be related to aluminium

distribution and location and further investigations should be done in order to elucidate the role of OSDA on the aluminium siting [39, 40].

Figure 6 depicts the FT-IR spectra of H-ferrierite samples before and after adsorption of deuterated acetonitrile. Fore bare samples, two main bands observed at 3745 cm^{-1} and 3600 cm^{-1} are associated with terminal silanol Si-OH and Brønsted acid sites Al-OH-Si groups, respectively [41, 42]. A shoulder at around 3645 cm^{-1} is also present. Similar result was reported already [28, 43], but the peak is not well-identified. Peixoto et al. [44] suppose that the observed shoulder can be associated to a silanol group anchored on extra-framework aluminium species (e.g., octahedral aluminium) as reported also by Rachwalik et al. [45] even though in the investigated samples, NMR analysis suggests that octahedral aluminium species are nearly absent. It is known from the literature that aluminium in highly distorted coordination might become NMR silent and the observed band at 3645 cm^{-1} can be associated to OH groups connected to the so called 'invisible' aluminium species [46, 47] that can play a role of Lewis acid sites [48, 49]. The presence of these species could explain the non-stoichiometric Na/Al ratio discussed above.

After adsorption of CD_3CN, two main bands at about 2296 cm^{-1} and 2322 cm^{-1} appear, revealing the presence of both Brønsted and Lewis acid sites, respectively, in boith cthe samples. Smaller bands at lower wave length associated with physisorbed acetonitrile are also presents [30]. The concentration of Brønsted and Lewis sites were obtained from the integral intensities of the IR bands of adsorbed CD_3CN at 2296 cm^{-1} and 2322 cm^{-1}, respectively, by using the extinction factor coefficients reported in Section 2. Brønsted and Lewis site distribution of the investigated samples was calculated from the

area of bands recorded at 25 °C; both the samples exhibits a significant amount (asround 40 %) of Lewis acid sites.

In order to estimate the strength of Brønsted and Lewis acid sites TPD measurements were carried out in the range 25-400 °C. Figure 7 shows both the FT-IR profiles and the fraction of Brønsted and Lewis acid sites free of adsorbed D_3CN molecules as a function of desorption temperature.

The set of data show that Lewis acid sites are stronger than Brønsted ones for all the samples. The desorption of Brønsted sites becomes significant above 150°C while the Lewis sites are still occupied above 300°C. In particular, the desorption of acetonitrile molecules starts at 50 °C and no occupied sites are present above 250 °C for both the samples, indicating a similar strength distribution. On the contrary, the desorption of probe molecules from Lewis acid sites starts above 25 °C and 150 °C for En-FER and DAO-FER, respectively. This result indicates that En-FER possesses weaker Lewis acid sites than DAO-FER. By considering as strong Lewis acid sites fraction, the value of Lewis acid sites still occupied by CD_3CN molecules at 300 °C, it is possible to calculate the fraction of strong Lewis sites reported in Table 2 (last column). DAO-FER possesses a higher amount of strong Lewis acid sites than En-FER, indicating that the synthesis system affects both typology and strength of acid sites.

3.3 DTF calculations

As previously discussed, 1,8-diaminooctane was never reported as a template for FER-type structure, to the best of our knowledge. Our data unambiguously show that DAO is incorporated in FER channels and fulfil the function of OSDA and charge balancing cation, similarly to the other nitrogen-SDA. This aspect was also addressed from a

theoretical point of view, by performing a DFT simulation for the investigated systems. In this regard, zeolite is considered as an infinite crystal and dispersion corrections are used in order to take into account confinement effects. Both binding energies and length of H(SDA)---O(FER) hydrogen bonds are reported in Table 3 and the optimized structures are displayed in Figure 8.

The binding of both En and DAO with the 10 MR pore walls of zeolite are thermodynamically favoured (i.e. negative binding energies are calculated) suggesting that SDAs bind though hydrogen-bond formations with the lattice of zeolite. In particular, the strong interaction energy calculated for En-FER system may be attributed to the short hydrogen bond lengths, that are also almost linear and therefore stronger than the other systems.

Similarly, DAO is stabilized in FER cavity via several short and linear N-H---O(ZEO) H-bonds, which explains, also in this case, the computed strong interaction energy with pore walls of FER zeolite. Furthermore, the computed dispersion energies for all the systems is about 0.3% to the total energy, indicating that the is not a particular stabilization of SDA molecules due to the attractive dispersion interactions or confinement effect. Concerning DAO-FER system, DFT calculations suggest that DAO molecules may be located in 10 MR channels of FER zeolite and that the formation of H-bond is the driving force for the stabilization of the molecules within the voids of zeolite. These results are in agreement with the chemical analysis. In fact, in the case of En, SDA molecules are protonated and they are able to compensate the negative charge of aluminium located in both 8 MR and 10 MR channels, and therefore, a low amount of sodium is required. On the contrary, if the accommodation of protonated SDA molecules within 8 MR channels is difficult, as in the case of DAO, more sodium is

415 required for compensating negative charge inside 8 MR channels. This conclusion is in
416 agreement with previous studies on ferrierite [50, 51].

417

418 **4. CONCLUSIONS**

419 In this work, for the first time, FER-type crystals were successfully synthesised by
420 using 1,8-diaminooctane (DAO) as organic structure directing agent (DAO-FER
421 sample). The obtained results in terms of crystals morphology and acidity were
422 discussed by taking FER zeolite prepared with ethylenediamine as reference (En-FER
423 sample). XRD analysis suggests that the presence of DAO reduces the induction time
424 respect to ethylenediamine, leading to the formation of smaller crystals with a lower
425 agglomeration. TG/DTA clearly indicates the presence of DAO inside the cavity of
426 zeolite, whilst chemical analysis suggest that protonated DAO is able to balance AlO_2^-
427 charge of the framework along 10 MR channels, while sodium shall be incorporated
428 along the 8 MR. On the contrary, a negligible amount of sodium is requested in the case
429 of ethylenediamine. In fact, DFT simulations show that DAO may be incorporated
430 along the 10 MR only, whilst ethylenediamine is able to balance the charges of Al
431 centres along both 8 and 10 MR channels. Furthermore, a higher amount of aluminium
432 is incorporated when DAO is used as OSDA leading to a higher total acidity. FT-IR
433 measurements reveal that both DAO- and En-FER samples possess a high amount of
434 Lewis acid sites (about 40%) that are stronger for DAO-FER sample.

435 The obtained results show the possibility to control the physicochemical properties of
436 zeolite crystals by selecting the type of structure directing agent leading to tailored
437 materials for specific applications, e.g. heterogeneous catalysis.

438

ACKNOWLEDGMENTS

The authors gratefully acknowledge Dr. Eddy Dib, Catalysis and Spectroscopy Laboratory LCS ENSICAEN, for NMR analysis.

REFERENCES

[1] A. Corma, J. Catal. 216 (2003) 298 – 312.

[2] B. M. Weckhuysen, J. Yu, Chem. Soc. Rev. 44 (2015) 7022

[3] F. Di Renzo, Catal. Today 41 (1998) 37-40.

[4] J. N. Armor, Catal. Today 163 (2011) 3-9

[5] S. Mintova, J.-P. Gilson, V. Valtchev, Nanoscale 5 (2013) 6693-6703.

[6] J. Pérez-Ramírez, C. H. Christensen, K. Egeblad, C. H. Chriestensen, J. C. Groen, Chem. Soc. Rev. 37 (2008) 2530-2542.

[7] V. Valtchev, G. Majano, S. Mintova, J. Pérez-Ramírez, Chem. Soc. Rev. 42 (2013) 263-290.

[8] W.-Q. Xu, Y.-G. Yin, S. L. Suib, J. C. Edwards, C.-L. O'Young, J. Phys. Chem. 99 (1995) 9443-9451.

[9] Y. Kamimura, C. Kowenje, K. Yamanaka, K. Itabashi, A. Endo, T. Okubo, Microp. Mesop. Mater. 181 (2013) 154-159.

[10] S. F. Abdo, S. T. Wilson, in: J. Cêjka, R. Morris, P. Nachtigall (Eds.), Zeolites in catalysis: properties and applications, The Royal Society of Chemistry, London, UK, 2017, RSC Catalysis Series 28, pp. 310-350.

[11] E. Catizzone, A. Aloise, M. Migliori, G. Giordano, Microp. Mesop. Mater. 243 (2017) 102-111.

[12] E. Catizzone, G. Bonura, M. Migliori, F. Frusteri, G. Giordano, Molecules, 23 (2018) 31-58.

[13] G. Bonura, M. Migliori, L. Frusteri, C. Cannilla, E. Catizzone, G. Giordano, F. Frusteri, J. CO_2 Util. 24 (2018) 398-406.

[14] P.S.S. Prasad, J.W. Bae, S. Kang, Y. Lee, K. Jun, Fuel Process. Technol. 89 (2008) 1281 – 1286.

[15] E. Catizzone, M. Milgiori, A. Purita, G. Giordano, J. Energ. Chem. 30 (2019) 162-169

[16] Y. Suzuki, T. Wakihara, K. Itabashi, M. Ogura, T. Okubo, Top. Catal. 52 (2009) 67-74

[17] Z. Gogebakan, H. Yucel, A. Culfaz, Ind. Eng. Chem. Res. 46 (2007) 2006-2012

[18] H. Gies, R.P. Gunawardane, Zeolites 7 (1987) 442-445.

[19] N.R. Forbes, L.V.C. Rees, Zeolites 15 (1995) 444-451

[20] R.A. Rakoczy, M. Breuninger, M. Hunger, Y. Traa, J. Weitkamp, Chem. Eng. Technol. 25 (2002) 273-275.

[21] R. A. Rakoczy, Y. Traa, P. Kortunov, S. Vasenkov, J. Kärger, J. Weitkamp, Microp. Mesop. Mater. 104 (2007) 179-184.

[22] Y. Lee, M. B. Park, P. S. Kim, A. Vicente, C. Fernandez, I.-S. Nam, S. B. Hong, ACS Catal. 3 (2013) 617-621.

[23] A. Kuperman, S. Nadimi, S. Oliver, G. A. Ozin, J. M. Garcés, M. M. Olken, Nature 365 (1993) 239-242.

[24] A.B. Pinar, L. Gómex-Hortiguela, L.B. McCusker, J. Pérez-Pariente, Chem. Mater. 25 (2013) 3654-3661.

[25] A.B. Pinar, C. Márquez-Álvarez, M. Grande-Casas, J. Pérez-Pariente, J. Catal. 263 (2009) 258-265.

[26] M. Derewinski, M. Machowska, Stud. Surf. Sci. Catal. 154 (2004) 349-354.

[27] G. Giordano, N. Dewale, Z. Gabelica, J. B. Nagy, E. G. Derouane, Appl. Catal. 71 (1991) 79-87.

[28] X. Chen, T. Todorova, A. Vimont, V. Ruaux, Z. Qin, J.-P. Gilson, V. Valtchev, Microp. Mesop. Mater. 200 (2014) 334-342.

[29] P. Lanzafame, G. Papanikolaou, S. Perathoner, G. Centi, M. Migliori, E. Catizzone, G. Giordano, Appl. Catal. A: Gen. 580 (2019) 186-196.

[30] B. Wichterlová, Z. Tvarůková, Z. Sobalík, P Sarv, Micropor. Mesopor. Mat. 24 (1998) 223 – 233.

[31] D. Vuono, L. Pasqua, F. Testa, R. Aiello, A. Fonseca, T.I. Korányi, J. B.Nagy, Micropor. Mesopor. Mat. 97 (2006) 78 – 87.

[32] N.R. Forbes, L.V.C. Rees, Zeolites 15 (1995) 444-451.

[33] N.R. Forbes, L.V.C. Rees, Zeolites 15 (1995) 452-459.

[34] L.D. Rollmann, J.L. Schlenker, S.L. Lawton, C.L. Kennedy, G.J. Kennedy, D.J. Doren, J. Phys. Chem. B 103 (1999) 7175-7183.

[35] M. Niwa, N. Katada, Chem. Rec. 13 (2013) 432 – 455.

[36] N. Katada, M. Niwa, Catal. Surv. Asia 8 (2004) 161 – 170.

[37] C.V. Hidalgo, H. Itoh, T. Hattori, M. Niwa, Y. Murakami, J. Catal. 85 (1984) 362-369.

[38] C. Costa, I.P. Dzikh, J.M. Lopes, F. Lemos, F.R. Ribeiro, J. Mol. Catal. A: Chem. 154 (2000) 193-201.

[39] N. Wang, M. Zhang, Y. Yu, Microp. Mesop. Mater. 169 (2013) 47-53

[40] D. Zhou, Y. Bao, M. Yang, N. He, G. Yang, J. Mol. Catal. A: Chem., 244 (2006) 11-19.

[41] Y.P. Khitev, Y.G. Kolyagin, I.I. Ivanova, O.A. Ponomareva, F. Thibault-Starzyk, J.-P. Gilson, C. Fernadez, F. Fajula, Microp. Mesop. Mater. 146 (2011) 201-207.

[42] J. Datka, M. Kawalek, K. Góra-Marek, Appl. Catal. A: Gen. 243 (2003) 293-299.

[43] P. Cañozares, A. Carrero, P. Sánchez, Appl. Catal. A: Gen. 190 (2000) 93-105

[44] D.P.B. Peixoto, S.M. Cabral de Menezes, M.I. Pais da Silva, Mater. Lett. 57 (2003) 3933-3942.

[45] R. Rachwalik, Z. Olejniczak, J. Jiao, J. Huang, M. Hunger, B. Sulikowski, J. Catal. 252 (2007) 161-170.

[46] A. Bonilla, D. Baudouin, J. Pérez-Remírez, J. Catal. 265 (2009) 170-180.

[47] C.P. Grey, A.J. Vega, J. Am. Chem. Soc. 117 (1995) 8232-8242.

[48] D. Verboekend, K.C. Groen, J. Pérez-Remírez, Adv. Funct. Mater. 20 (2010) 1441-1450.

[49] F. Deng, Y. Yue, C. Ye, Solid State Nucl. Magn. Reson. 10 (1998) 151-160.

[50] L. Domokos, L. Lefferts, K. Seshan, J.A. Lercher, J. Mol. Catal. A: Chem, 162 (2000) 147-157.

528 [51] P. Sarv, B. Wichterlová, J. Čejka, J. Phys. Chem. B, 102 (1998) 1372-1378.

529

TABLES CAPTIONS

Table 1 Chemical composition, pore volume and surfaces characteristics of synthesised FER-type materials.

Table 2 Acidic properties of investigated catalysts.

Table 3 Calculated binding energies and lengths for the investigated SDA-FER systems from DFT simulation

538 **FIGURES CAPTIONS**

539 **Figure 1** XRD pattern of FER samples synthesized with ethylenediamine and 1,8-
540 diaminooctane (DAO). (*****) indicates the presence of Kaetite phase.

541 **Figure 2** TGA (continuous line) and dTG (dashed line) data of FER samples
542 synthesised with DAO/En=0 (A), DAO/En=0.5 (B), DAO/En=2 (C) and
543 DAO/En=∞ (D).

544 **Figure 3** N_2 adsorption (closed circle) and desorption (open circle) isotherms at 77
545 of En-FER and DAO-FER samples.

546 **Figure 4** SEM micrographs of FER-type materials synthesised with
547 ethylenediammine and 1,8-diaminooctane.

548 **Figure 5** NH_3-TPD profiles of En-FER and DAO-FER samples.

549 **Figure 6** FT-IR spectra of of En-FER and DAO-FER samples after evacuation at
550 300 °C for 4h (a) and after adoption of CD_3CN molecules at 25°C (b).
551 All the spectra are recorded at 10^{-6} torr.

552 **Figure 7** FT-IR spectra of D_3-acetonitrile adsorbed on En-FER (A), and DAO-
553 FER (B) evacuated at 25 °C (a), 50 °C (b), 100 °C (c), 150 °C (d), 200
554 °C (e), 250 °C (f) and 300 °C (g). Fraction of Brønsted (●) and Lewis (■)
555 acid sites free of adsorbed D_3CN molecules as a function of desorption
556 temperature for En-FER (A') and DAO-FER(B').

557 **Figure 8** DFT optimized crystal structures of FER with SDA molecules. SDA in
558 10 MR and in 8 MR are shown in the top and down panels, respectively,
559 in Figs. a, b, c. Optimized unit cells structures of every FER-SDA are
560 displaced at the left-side and 2x2x2 cells - at the right side in Figs. a, b, c

and d. The dashed lines indicate all the H-bonds ≤ 3 Å. The lengths of the shorter and linear H-bonds bellow 2.5 Å are reported in Table X. Atomic colour code: dark blue for Si; red for O; light blue for $Al3^{+}$, black for C, violet for N, grey for H and yellow for Na.

SAMPLE	En-FER	DAO-FER
Na/Al_{bulk}[a] [mol/mol]	0.06	0.60
Si/Al_{bulk}[a] [mol/mol]	8.4	6.6
S_{BET}[b] [m^2/g]	329	287
V_{mic}[c] [cm^3/g]	0.131	0.125

[a] Atomic absorption

[b] BET superficial area

[c] Micropore volume calculated by *t*-plot method

Table 1

	En-FER	DAO-FER
NH_3-uptake [$\mu mol/g_{cat}$]	1052	1418
$T_{M,LT}$[a] [°C]	245	231
x_{LT}[b]	0.30	0.40
$T_{M,HT}$[c] [°C]	436	455
x_{HT}[d]	0.70	0.60
Lewis acid sites[e] [%]	0.41	0.40
Strong Lewis acid sites[f] [%]	0.16	0.24

[a] Temperature of maximum desorption of NH_3 between 100 and 300°C

[b] Fractional population of sites between 100 and 300°C

[c] Temperature of maximum desorption of NH_3 above 300°C

[d] Fractional population of sites above 300°C

[e] Estimated by FT-IR analysis of adsorbed D_3-acetonitrile at 25°C

[f] Estimated by FT-IR analysis of adsorbed D_3-acetonitrile at 300°C

Table 2

Sample	*Binding energy (eV/mol)*		*Binding lengths (Å)*	
	8 MR	10 MR	8 MR	10 MR
En-FER	-24.01	-25.76	1.820 1.908 1.710	1.864 1.902 2.473
DAO-FER	N.a.N	-22.67	-	2x1.960; 2.042[a] 2.129; 1.498[b] 2.441, 2.488[c]

[a] NH_3^+---O(ZEO) H-bond;
[b] NH_2---O(ZEO) H-bond
[c] C(CH)---O(ZEO) H-bond

Table 3

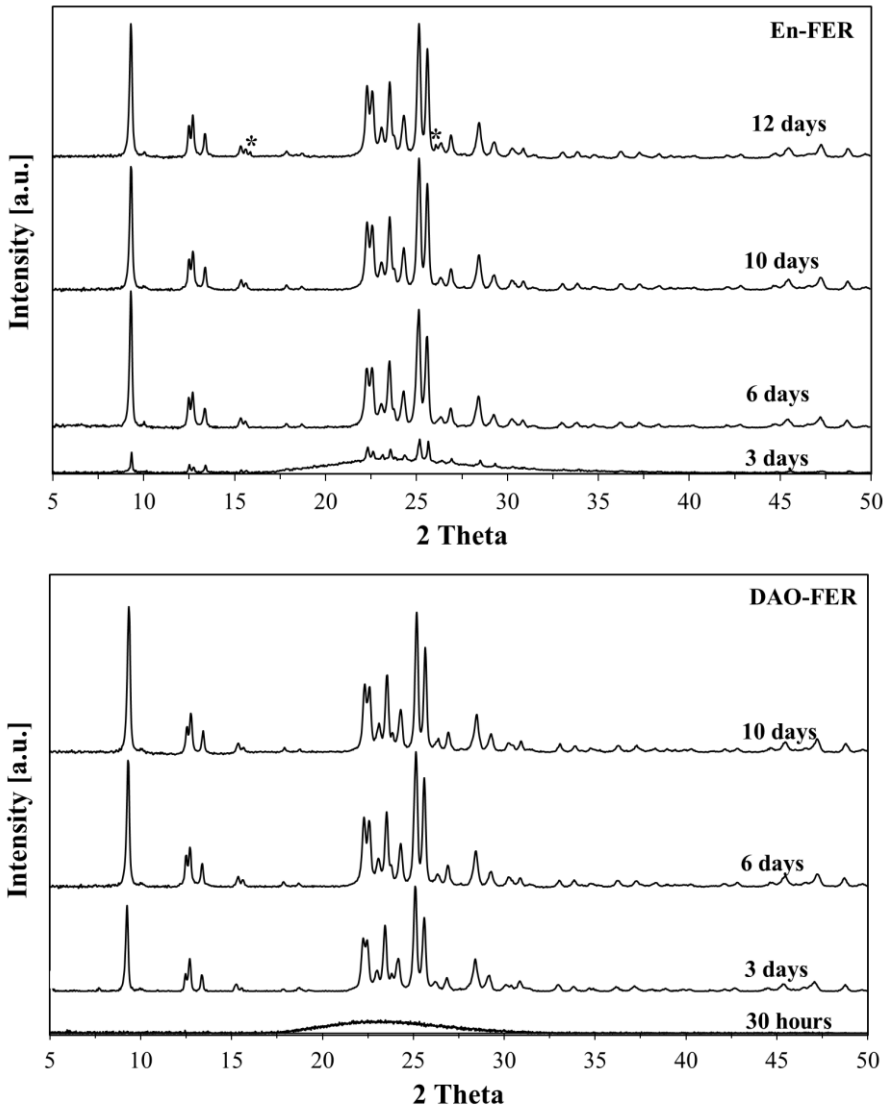
En-FER
12 days
10 days
6 days
3 days
Intensity [a.u.]
2 Theta
DAO-FER
10 days
6 days
3 days
30 hours
Intensity [a.u.]
2 Theta

Figure 1

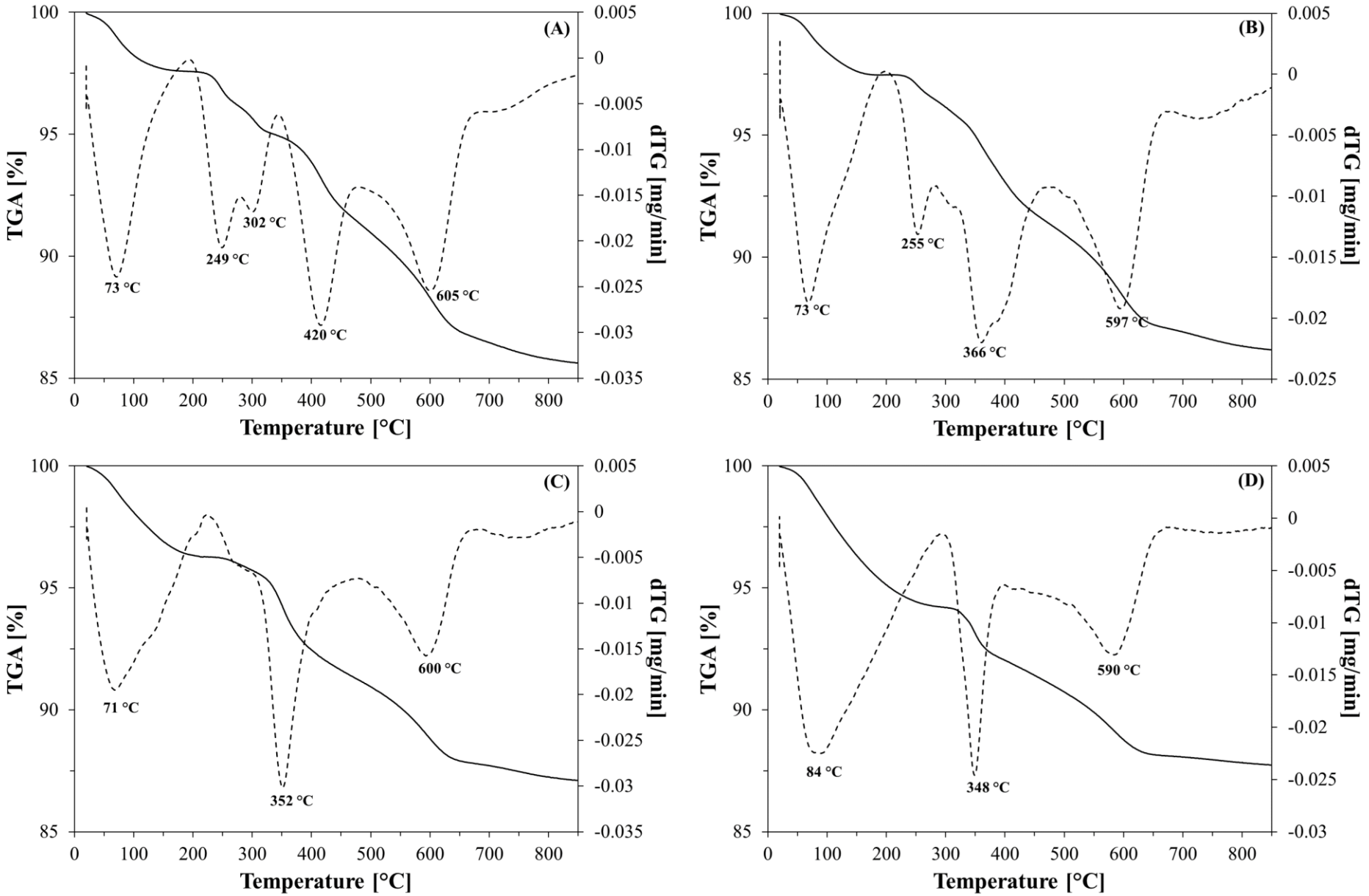
(A)
TGA [%]
dTG [mg/min]
Temperature [°C]
73 °C
249 °C
302 °C
420 °C
605 °C
(B)
TGA [%]
dTG [mg/min]
Temperature [°C]
73 °C
255 °C
366 °C
597 °C
(C)
TGA [%]
dTG [mg/min]
Temperature [°C]
71 °C
352 °C
600 °C
(D)
TGA [%]
dTG [mg/min]
Temperature [°C]
84 °C
348 °C
590 °C

Figure 2

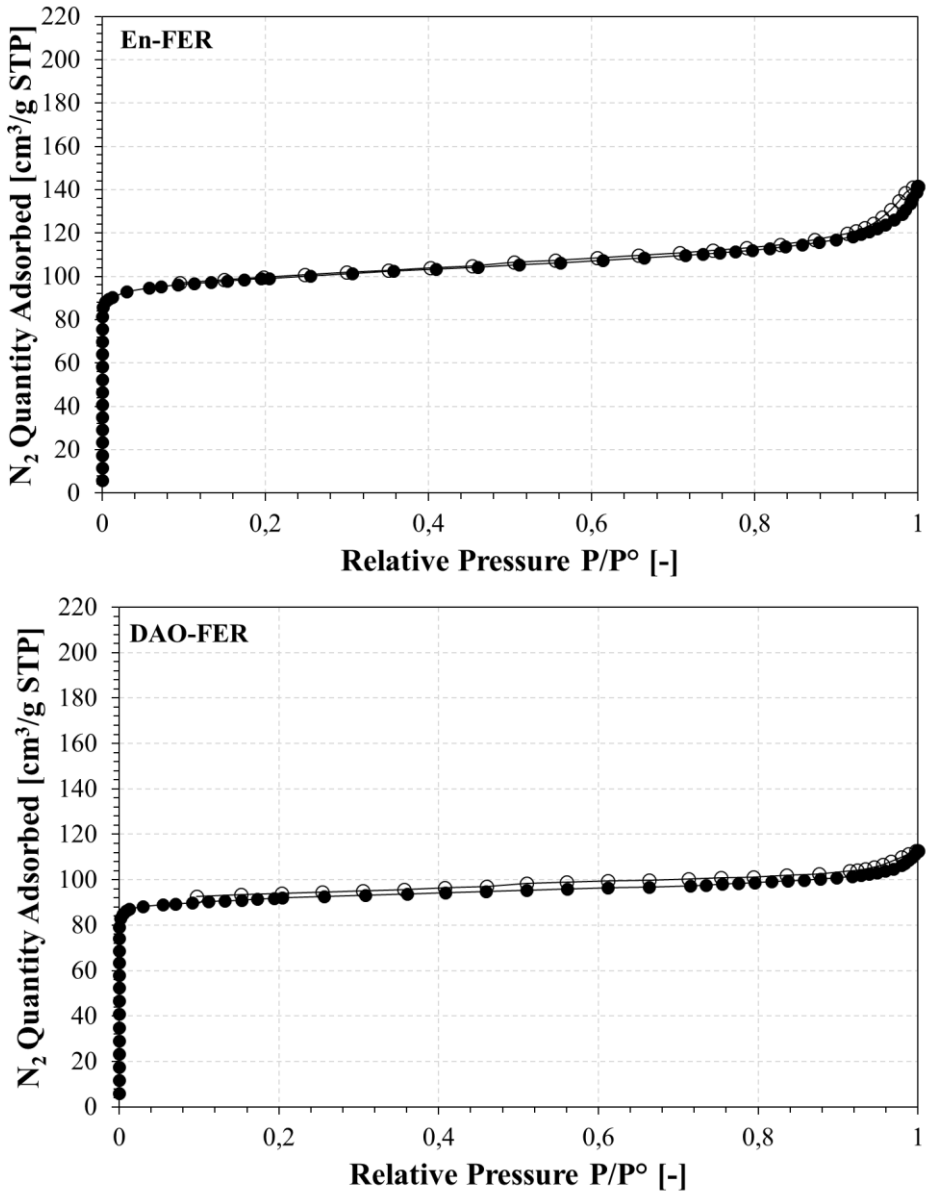
En-FER
N2 Quantity Adsorbed [cm3/g STP]
Relative Pressure P/P° [-]
DAO-FER
N2 Quantity Adsorbed [cm3/g STP]
Relative Pressure P/P° [-]

Figure 3

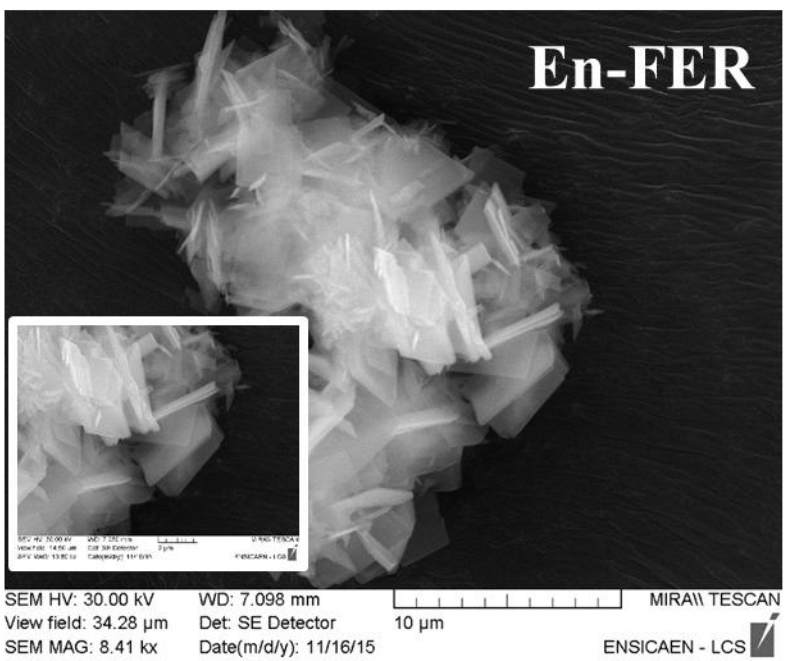
En-FER
SEM HV: 30.00 kV
WD: 7.098 mm
MIRA\\ TESCAN
View field: 34.28 µm
Det: SE Detector
10 µm
SEM MAG: 8.41 kx
Date(m/d/y): 11/16/15
ENSICAEN - LCS

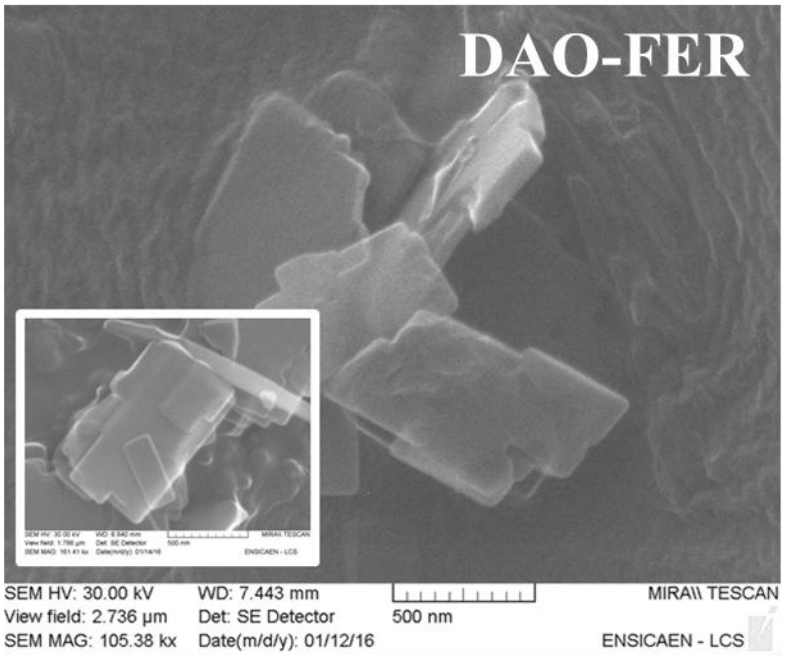
DAO-FER
SEM HV: 30.00 kV
WD: 7.443 mm
MIRA\\ TESCAN
View field: 2.736 µm
Det: SE Detector
500 nm
SEM MAG: 105.38 kx
Date(m/d/y): 01/12/16
ENSICAEN - LCS

Figure 4

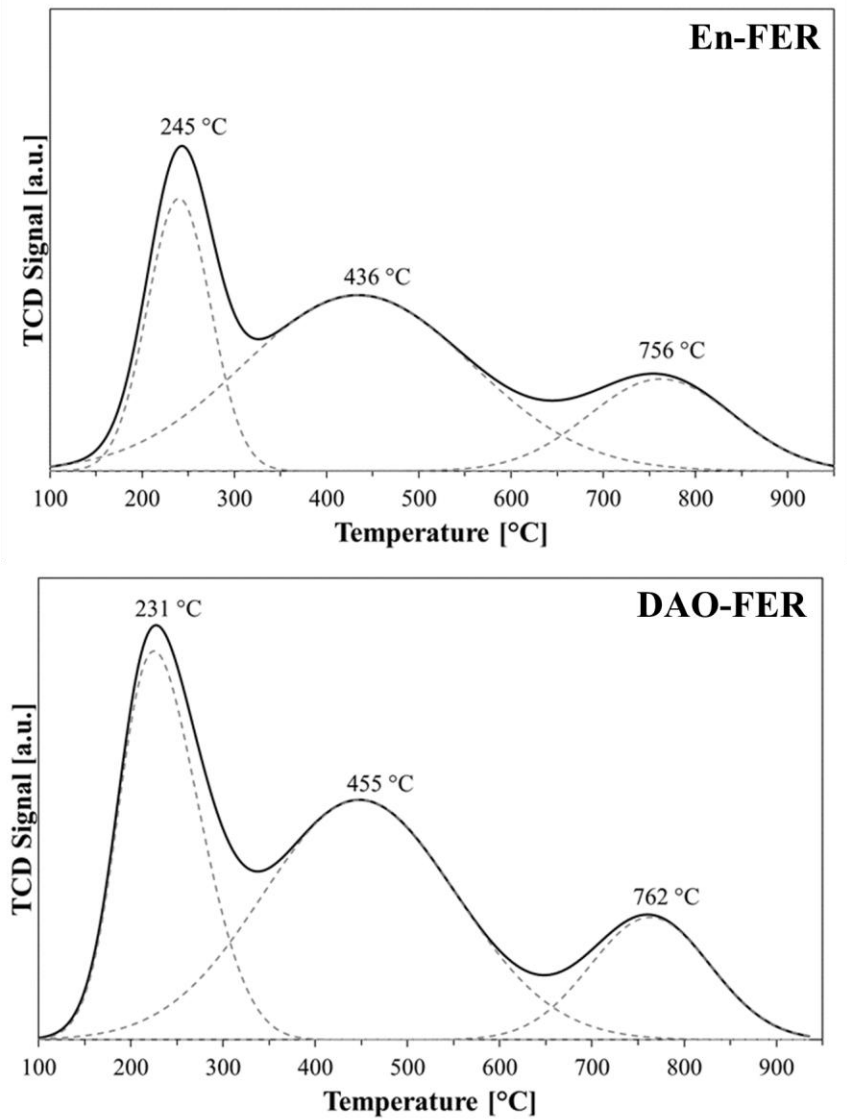
En-FER
245 °C
436 °C
756 °C
TCD Signal [a.u.]
100
200
300
400
500
600
700
800
900
Temperature [°C]
DAO-FER
231 °C
455 °C
762 °C
TCD Signal [a.u.]
100
200
300
400
500
600
700
800
900
Temperature [°C]

Figure 5

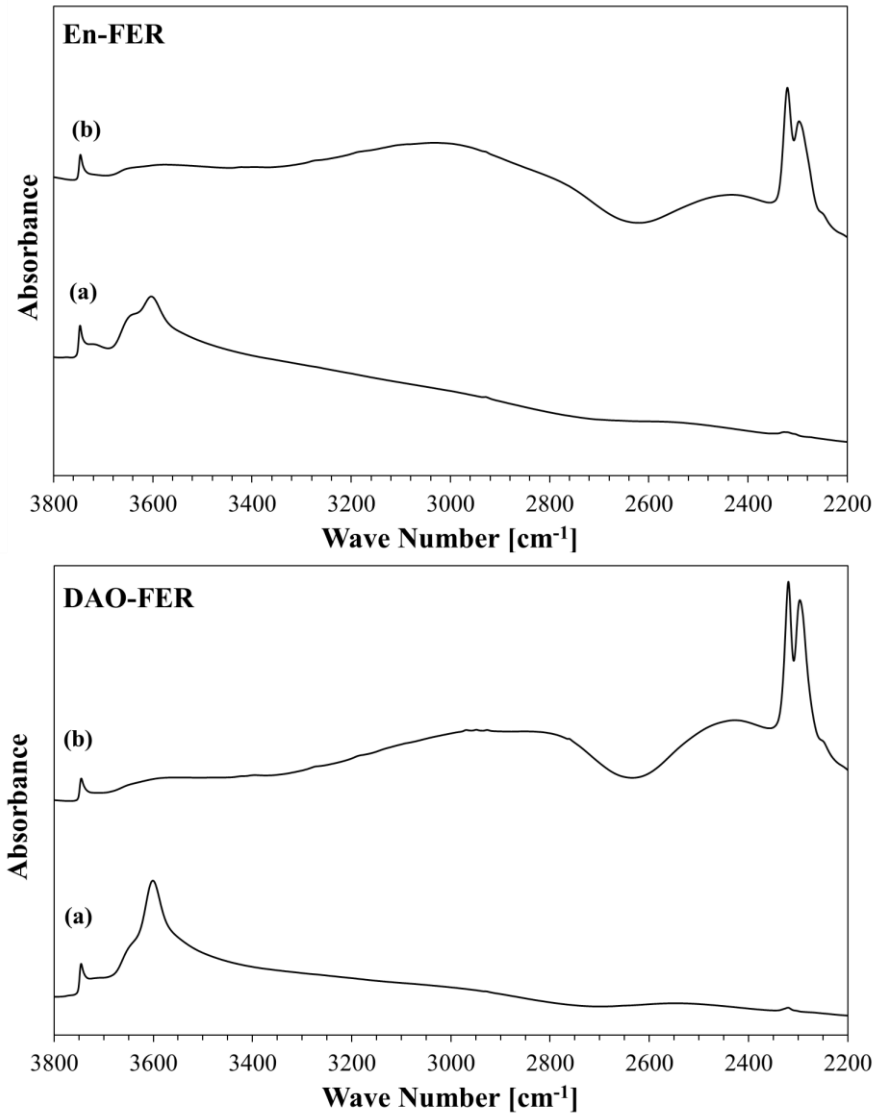
En-FER
(b)
(a)
Absorbance
3800
3600
3400
3200
3000
2800
2600
2400
2200
Wave Number [cm-1]
DAO-FER
(b)
(a)
Absorbance
3800
3600
3400
3200
3000
2800
2600
2400
2200
Wave Number [cm-1]

Figure 6

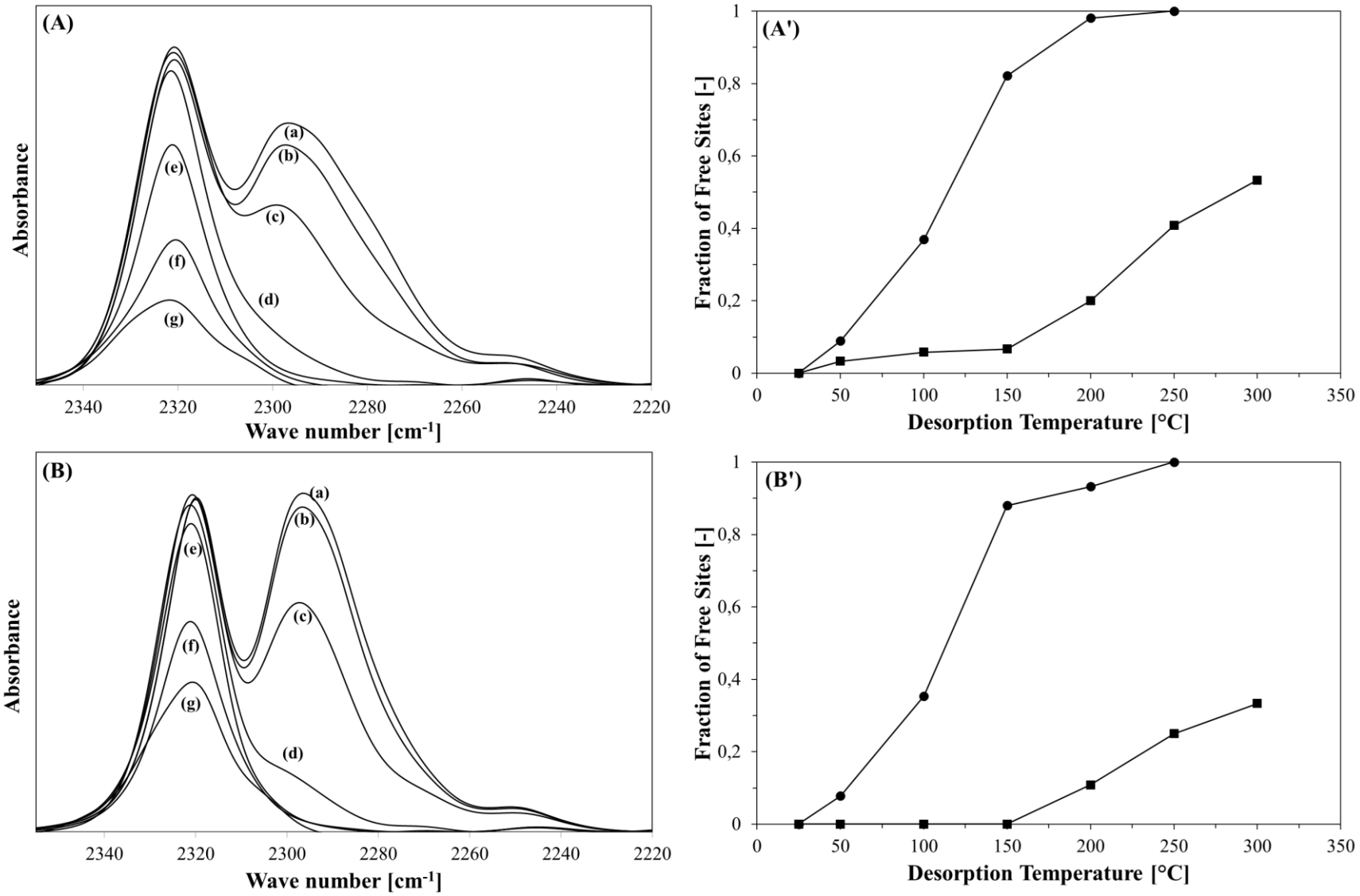
(A)
Absorbance
(a)
(b)
(c)
(d)
(e)
(f)
(g)
2340
2320
2300
2280
2260
2240
2220
Wave number [cm-1]
(A')
Fraction of Free Sites [-]
0
0,2
0,4
0,6
0,8
1
0
50
100
150
200
250
300
350
Desorption Temperature [°C]
(B)
Absorbance
(a)
(b)
(c)
(d)
(e)
(f)
(g)
2340
2320
2300
2280
2260
2240
2220
Wave number [cm-1]
(B')
Fraction of Free Sites [-]
0
0,2
0,4
0,6
0,8
1
0
50
100
150
200
250
300
350
Desorption Temperature [°C]

Figure 7

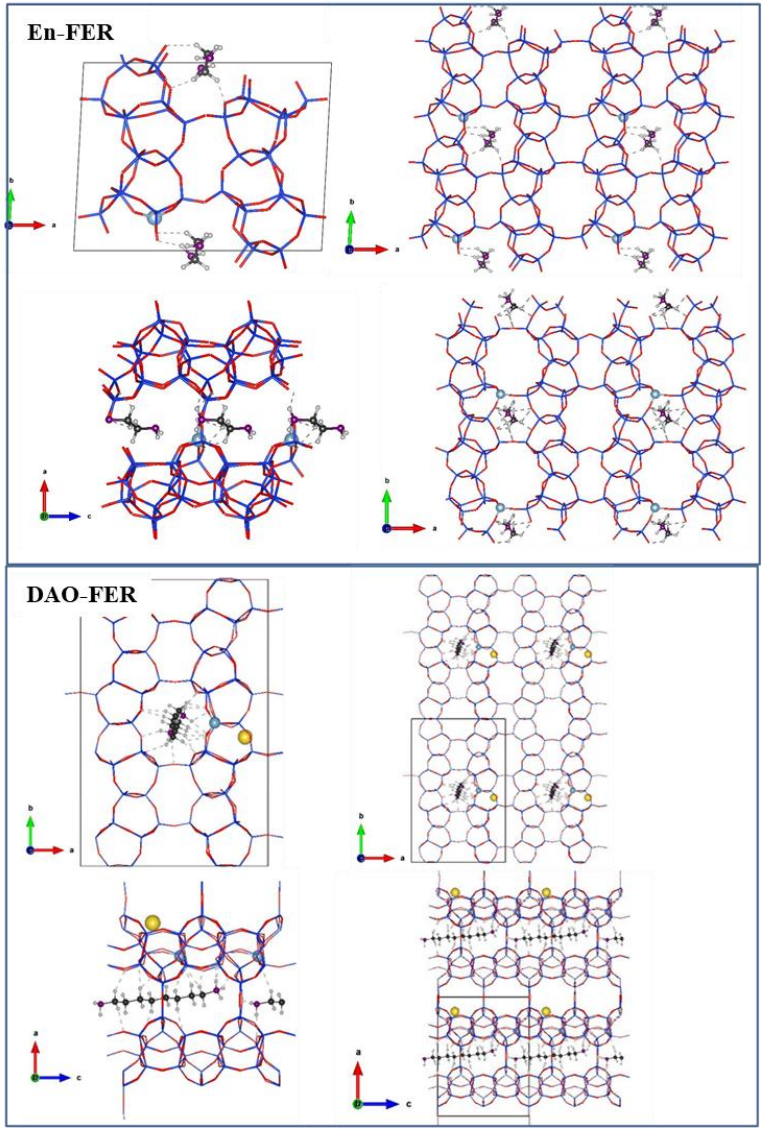

Figure 8